*Annual Review of Fluid Mechanics*

# Vortex-Induced Vibration of Flexible Cylinders in Cross-Flow

Francisco Huera-Huarte

Department of Mechanical Engineering, Universitat Rovira i Virgili, Tarragona, Spain; email: francisco.huera@urv.cat



Annu. Rev. Fluid Mech. 2025. 57:285–310

First published as a Review in Advance on September 30, 2024

The *Annual Review of Fluid Mechanics* is online at fluid.annualreviews.org

https://doi.org/10.1146/annurev-fluid-022724-014235



## Keywords

flow-induced vibrations, flexible circular cylinders, multimode and multifrequency vortex-induced vibration

## Abstract

This review provides a comprehensive analysis of the literature on vortex-induced vibration (VIV) of flexible circular cylinders in cross-flow. It delves into the details of the underlying physics governing the VIV dynamics of cylinders characterized by low mass damping and high aspect ratio, subject to both uniform and shear flows. It compiles decades of experimental investigations, modeling efforts, and numerical simulations and describes the fundamental findings in the field. Key focal points include but are not limited to amplitude–frequency response behavior, the relationship between the distributed loading acting on the cylinder and the trajectories and the near wake structures around the cylinder, the existence of traveling waves, the identification of power-in/power-out regions, and the modal overlapping and mode competition phenomena.

## 1. INTRODUCTION

**Mass ratio:** the ratio of structural mass to fluid mass, $m^* = 4m/\rho\pi LD^2$

The study of vortex-induced vibration (VIV) stands as a pivotal area of research that has profound implications, not only academically in the fields of fluid mechanics and structural dynamics, but also across diverse engineering domains. VIV occurs when fluid flow induces oscillatory motion in flexibly mounted rigid structures or in flexible systems, driven by the vortex shedding in its wake. When the mass ratio (the ratio of structural to fluid mass) is small, the coupling between the shedding and the dynamics of the structure is especially complex (Bearman 1984, Blevins 1990, Sarpkaya 2004, Williamson & Govardhan 2004, Naudascher & Rockwell 2005, Bearman 2011, Païdoussis et al. 2014).

VIV has generated great interest within the industry because of its practical implications. Its relevance spans various critical engineering systems exposed to wind or water currents such as chimneys and stacks, high-rise structures, constructive elements of bridges, heat exchangers, power transmission lines, pipelines, drilling and production risers, spar hulls and other offshore structures, marine cables, tendons and mooring lines, tethers, and so on. In the field of ocean engineering, where mass ratios are low and the dynamics becomes very rich, the industry has shown particular interest over the past decades. **Figure 1*a*** shows a flexible cylinder idealization of the tendons in a multicolumn floating offshore wind turbine platform as an example. In these scenarios, VIV is of extreme importance as it can significantly affect the performance and structural integrity of offshore systems, leading to large-amplitude oscillations with clashing between structures, fatigue, and other critical types of failure. Understanding the behavior of flexible cylinders under VIV conditions is paramount for optimizing the design and operation of engineering systems subjected to fluid flow, particularly in scenarios where slender structures and deep waters are a must. For reference, until 1985 the maximum water depth in the existing operational oil

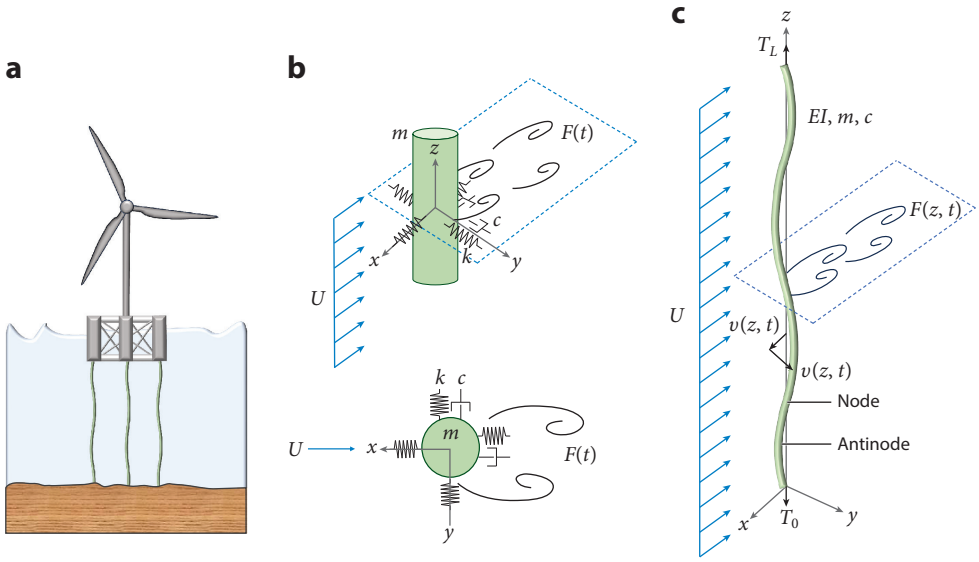


**Figure 1**

(*a*) Representation of an offshore wind turbine on top of a multicolumn tension leg platform. (*b*) Parts of this type of system have been traditionally modeled as flexibly mounted rigid cylinders with either one or two degrees of freedom. (*c*) Tendons and other slender offshore structures can be idealized using a vertical flexible cylinder in cross-flow with certain mechanical characteristics.

wells was approximately 500 m, but during the following decade, water depths started to become larger and larger, surpassing 1,800 m. In actual developments in the Gulf of Mexico, maximum water depths have reached 2,950 m (Bur. Ocean Energy Manag. 2019). One can imagine the harsh environments and the complex water currents that these structures face during operation. In all these scenarios, the flexible cylinder is a canonical model for the study of VIV in elastic structures affected by a cross-flow.

**Aspect ratio:** the ratio of the length of the structure to its diameter, $L/D$

Experiments have been widely used to study VIV in the past, not only as the main way to advance the understanding of physics, but also to produce data to validate the rapidly developing numerical codes in recent decades. The design of experiments involving flexible cylinders is always a challenging problem, as it generally requires large facilities even when reduced-scale models are used. Deepwater riser pipes can have lengths well over several hundred meters; therefore, reduced-scale versions of these and other slender structures for laboratory experiments can end up being very large in order to achieve dynamic similarity. Supporting and auxiliary structures used to hold the models in the facilities end up being large and expensive, and they need to be carefully designed in order to have natural frequencies far from the expected excited ones during the experiments. One of the major problems is that, in order to measure the dynamics of long elastic vibrating cylinders, there is a need for a large number of measurement stations along the length of the cylinder. Moreover, the aspect ratio (the ratio of length to diameter) needs to be large enough to promote an adequate proportion between the high-mode-number wavelengths and the dimensions of the model. The ideal number of equally spaced measurement stations coincides with the mode number to be resolved, although it has been shown that a limited number of nonequidistant sensors can also lead to high mode shape reconstruction (Mukundan et al. 2010, Seyed-Aghazadeh & Modarres-Sadeghi 2016).

In field experiments, i.e., tests in open waters or in the ocean environment, it is not always possible to instrument the structural members with the appropriate number of sensors, and therefore some of the results obtained are limited and lack generality. Measurements need to be nonintrusive, so typical sensor technologies used to instrument models for laboratory experiments are accelerometers, strain gauges, and fiber Bragg gratings and other optical tracking techniques. While optical techniques are completely nonintrusive and directly provide the displacements along the length of the model, other measurement techniques require not only the installation of sensors (and cables) on the model, but also numerical procedures to indirectly obtain the motion.

Of extreme importance are the loads seen by the model due to the complex fluid–structure interaction phenomena. The measurement of the total forces, i.e., drag (in-line to the flow force) and lift (transverse to the flow force), is a relatively straightforward task if dedicated sensors are used at the ends of the cylinder, where they are attached to the supporting structures. Mean drag forces can also be computed using beam deflection analytical solutions or numerical methods by using measured mean static deflections to obtain forces. More difficult is the nonintrusive measurement of the time-dependent localized dynamic forces along the length of these high-aspect-ratio structures. This would imply the nonintrusive measurement of the force acting on the cylinder at many different points along the length. In fact, to the knowledge of the author, there are no experimental, time-varying force distribution direct measurements along the length of long flexible cylinders available in the literature. In the past, inverse numerical methods were used as the only way to deal with the ill-posed problem of obtaining the distributed loading from the measured response. The forcing is the result of the complex fluid dynamics around and along the length of the vibrating cylinder model, which is also very difficult to measure. Experiments using optical interrogation techniques such as digital particle image velocimetry (DPIV) (Willert & Gharib 1991) have been done in the past, but these usually lead to local planar flow fields at

different points along the length, making the three-dimensional reconstruction of the flow very difficult. Recent advancements in numerical simulation have significantly improved the capacity to resolve flow dynamics in detail. This progress is enabling researchers to bridge the gap between numerical predictions and the experimental observations made over the past few decades.

This critical review examines both experimental and numerical investigations published over more than 40 years of research, to assess the current state of knowledge in the field. The emphasis is on a critical discussion of the physics and the results available in the literature, rather than the techniques used to obtain them. It offers valuable insights into the advancements made in the understanding of VIV of flexible circular cylinders in cross-flow. The article is organized as follows: In Section 2, the importance and the need for continuous models to study the VIV of flexible cylinders are emphasized. In Section 3, the main features associated with the hydrodynamic loading acting on flexible cylinders and their dynamic response are discussed for uniform and sheared flows. Finally, in Section 4, the flow dynamics and the wake structures identified in this type of problem are discussed.

**Strouhal number:** relates the shedding frequency to the free-stream velocity using a characteristic length, $S = f_s D/U$

**Reduced velocity:** the ratio of the free-stream flow velocity to a velocity scale related to the natural frequency of the structure in air or in water, $U^* = U/fD$

**Reynolds number:** the ratio of inertial to viscous effects, $Re = \rho UD/\mu$

## 2. FLEXIBLE CYLINDERS

The main features associated with the VIV of flexibly mounted rigid cylinders with one or two degrees of freedom are well understood and described in the vast literature available in the field. The two-dimensional model of a flexibly mounted rigid cylinder with one degree of freedom is characterized by mass ($m$), stiffness ($k$), and damping ($c$), as in the two schematic views shown in **Figure 1*b***. This model yields a differential equation, for the motion of the cylinder ($y$), of the form $m\ddot{y} + c\dot{y} + ky = F(t)$. The natural frequency of the system $f$ is given by $(2\pi)^{-1}\sqrt{k/m}$. The fluid loading is in general modeled using a harmonic expression of the form $F(t) = F_0 \sin(2\pi f_s t + \phi)$, which represents the alternating lift force acting on the system, where $f_s$ is the vortex shedding frequency and $\phi$ is the phase difference between displacement and force. The Strouhal number $S$ relates the shedding frequency to the free-stream velocity by means of the diameter of the cylinder. The response of such systems is usually characterized by studying the amplitude ($A^*$, in dimensionless form, referenced to $D$) and frequency ($f^*$, in dimensionless form, referenced to $f$) as a function of reduced velocity ($U^*$, the ratio of the free-stream flow velocity to a velocity scale related to $f$) and/or the Reynolds number ($Re$, the ratio of inertial to viscous effects). Different regions of response have been observed, namely initial, upper, lower, and desynchronization branches (Williamson & Govardhan 2004). Two-dimensional models have been used not only to study the VIV of rigid bodies, but also in the past to study the flexible cylinder problem, considering a cross-sectional view of it. It is clear, however, that many of the features associated with the flexible cylinder problem can be only understood by using continuous models. In fact, the question of how similar the dynamic response of flexible cylinders is to that of flexibly mounted rigid ones has been a recurring debate over the last decades, as discussed by Ma et al. (2022a).

A flexible cylinder has an infinite number of natural frequencies ($f_n$) and mode shapes ($\Theta_n$) and hence, intrinsically, it poses a more complicated problem, not only structurally, but also from the fluid–structure interaction point of view. Consider the elastic cylinder depicted in **Figure 1*c*** subject to a generic flow profile characterized by a free-stream velocity $U$. Typically, in the context of VIV, it is modeled using the Euler–Bernoulli beam equation (Han et al. 1999), which neglects transverse shear and rotary inertia and assumes all the fluid forces $F(z, t)$ to act parallel to the $x$ or $y$ direction,

$$m\frac{\partial^2 u(z,t)}{\partial t^2} + c\frac{\partial u(z,t)}{\partial t} + EI\frac{\partial^4 u(z,t)}{\partial z^4} - \frac{\partial}{\partial z}\left(T(z)\frac{\partial u(z,t)}{\partial z}\right) = F(z,t). \quad 1.$$

In the above equation, $u(z, t)$ is the transverse deflection along the length of the cylinder (in either the $x$ or $y$ direction). The mass $m$, usually considered constant in the $z$ direction, includes the added mass that results from the fact that the body needs to accelerate the surrounding fluid when vibrating, and it is usually expressed as a virtual mass of displaced fluid or as a function of the added mass coefficient ($c_m$). Flexural stiffness $EI$ and structural damping $c$ are usually considered to be constant along the length $L$, whereas tension $T$ can vary depending on the specific spatial configuration. Different boundary conditions can be applied, but the simply supported condition (zero displacements and curvatures at the ends) is probably the most common in the literature. If Equation 1 is used to describe an eigenvalue problem related to the dynamics of the simply supported generic long flexible cylinder with constant tension, one obtains the expression (Huera-Huarte & González 2013)

$$(m\lambda^2 + c\lambda)u + EI\frac{\mathrm{d}^4u}{\mathrm{d}z^4} - T\frac{\mathrm{d}^2u}{\mathrm{d}z^2} = 0, \qquad 2.$$

where the eigenvalues are the values of $\lambda$ that lead to nontrivial solutions of the equation, with the boundary conditions applied. Natural frequencies ($f_\mathrm{n}$) result from the imaginary part of the eigenvalues and are of the form

$$f_\mathrm{n} = \frac{n}{2}\sqrt{\left(n^2\pi^2\frac{EI}{mL^4} + \frac{T}{mL^2}\right)}, \qquad n = 1, 2, 3\ldots, \qquad 3.$$

with $n$ being the mode number. When tension dominates, natural frequencies grow linearly with the mode number, as an integer multiple of the natural frequency of the fundamental mode, being equally spaced from each other. This happens in the plane parallel to the flow as well as in the transverse one; therefore, resonance in both directions can take place depending on excitation, increasing the complexity of the problem even more. The growth of the natural frequencies is also inversely proportional to the length of the model [$\propto \sqrt{\frac{T}{m}}(\frac{n}{L})$]. In a bending stiffness–dominated case, natural frequencies grow quadratically with mode number and are inversely proportional to the square of the length [$\propto \sqrt{\frac{EI}{m}}(\frac{n}{L})^2$], so for a given length, the modal density is much lower at high modes than at low modes. It is in fact the aspect ratio ($L/D$) that relates tension and bending stiffness through the sectional inertia, dependent on $D$.

To date, a clear definition of what can be considered a flexible cylinder, in the context of VIV, is still missing. Structurally speaking, it is evident that a flexible body is such that it is not infinitely stiff, so it can deform and therefore can respond dynamically with different vibrational modes when perturbed. Modes are characterized by a certain number of nodes (regions with zero displacement amplitude during vibration) and antinodes (regions with maximum displacement amplitude during vibration), which can take place both in-line and transverse to the flow directions (see **Figure 1*c***). Experiments by Huera-Huarte & Bearman (2009a) showed that although the simply supported low-mass-damping cylinder model was flexible, some of the characteristics of the response for low-tension cases resulted in a response typical of flexibly mounted rigid models with a large response bandwidth, mainly because of the low aspect ratio. With increased tensions the response bandwidth was smaller, and the system started to depart from that behavior, with the desynchronization and lower branches (Williamson & Govardhan 2004) that are found in the VIV of flexibly mounted rigid cylinders practically vanishing. Other experiments with different flexible cylinder configurations and end conditions have shown similar trends (Sanaati & Kato 2012, Shang et al. 2014).

A flexible cylinder should be understood, in the context of VIV, as a cylinder, whether tension or bending dominated, with a large enough aspect ratio to produce a high modal density or mode count (Xie et al. 2004). This condition can ultimately lead to a multimode and multifrequency

dynamic response, characterized by a succession of lock-in states at different modes for different reduced velocities, with the presence of traveling waves and with a modal response that can show overlapping of modes and mode switches, depending on the characteristics of the incident flow. These aspects are discussed in detail in the following section.

## 3. LOCK-IN, DYNAMIC RESPONSE, AND HYDRODYNAMIC COEFFICIENTS

The process of lock-in (Bearman 1984) is of extreme importance in the dynamics of VIV. Lock-in is defined as the condition in which the excitation frequency is near one of the natural frequencies of the cylinder, and as a result, the response is mainly dominated by a certain mode that exhibits large-amplitude antinodal vibrations and increased drag forces. The structure governs the vortex shedding process, allowing large response amplitudes to occur not only in strict resonance conditions but also in a bandwidth around the classical resonant frequency. Low mass ratios have been found to play a role in widening response bandwidths as a result of a self-adaptation of the natural frequencies of the structure, through the varying added mass, that depends on the motion of the model itself.

A series of field experiments with long flexible circular cylinders in the 1980s (Vandiver & Jong 1987) resulted in one of the earliest data collections of VIV responses available in the literature. The authors conducted several experiments with models instrumented with biaxial accelerometers to study the relationship between cross-flow and in-line VIV responses or between lift and drag forces, which is important for fatigue estimation. They analyzed the response under lock-in conditions, with their model exhibiting figure-of-eight trajectories and a relatively narrow banded spectra, although at that time, with the available data, they were not able to fully reconstruct the modes and the mode shapes at which the model was responding. Under non-lock-in conditions, they observed random fluctuations of the amplitude and frequency, together with a wide banded lift and drag force spectra. One of the main findings reported in that work was the existence of a strong quadratic correlation between the cross-flow and the in-line vibration. Based on previously obtained data, Vandiver (1993) discussed the parameters that most heavily influenced the appearance or not of lock-in. Another significant question addressed in that research was related to the degree of dependency of the wake–structure synchronization process on variations in the incoming flow. Two parameters were proposed as the most important in determining the ability of a structure to lock in or not. The first was the number of modes falling inside a certain bandwidth and the second was the shear fraction of the flow. The damping ratio was said to play an important role in determining the lock-in response amplitudes, especially the relationship between structural and hydrodynamic damping in the different parts along the length of the system. The model was found to behave like a cable when large mode number response and high values of damping were present. The author defined the $n\xi$ parameter, resulting from the product of the modal damping ratio ($\xi$) and mode number, that seemed to be a good indicator for the ease of the system to experience lock-in conditions. Later on, Vandiver et al. (1996) analyzed the data from experiments conducted with a flexible cylinder in a stepped current with and without shear. The authors reported that in all the cases observed in their experiments with uniform flow, the response was dominated by a single lock-in mode. The number of sensors in these experiments was not enough to resolve high mode numbers and the observations were made after basic frequency domain analysis of the available data. It is shown in this section that multimode response can be found even in cases where lock-in clearly exists with spectra showing a single dominant frequency. In cases with sheared flows, the response varied depending on the amount of shear, and they identified single-mode lock-in cases, even with a strong shear in the incoming flow. These

early experimental works raised a large number of questions that have profoundly influenced subsequent research. They were also the starting point for the development of a series of prediction tools oriented to industry, such as SHEAR7 (Vandiver 2003), VIVA (Triantafyllou et al. 1999), and VIVANA (Larsen et al. 2005), that have been widely used by the industry to include VIV problems in the design of offshore developments.

Although shear is inherent to natural wind and water currents and therefore to engineering applications, uniform flows (see Section 3.1) have been studied as the starting point for the systematic study of VIV in flexible cylinders, at least in laboratory environments. In a uniform free stream, excitation is expected to happen at a single frequency, whereas with shear (see Section 3.2), the excitation frequency varies along the length of the cylinder. The generation of controlled shear in laboratories for high-mode-number VIV experiments is very challenging and it is restricted to large rotating arm facilities. Conversely, in field experiments, with shear always present, the problem is the correct characterization of the free stream and therefore the excitation. In the following sections, we delve into the knowledge accumulated over recent decades for the case of uniform (see Section 3.1) and shear (see Section 3.2) flows, concerning the factors governing lock-in and its interplay with added mass, the presence of standing or traveling waves, VIV amplitude and frequency responses, trajectory characteristics including their $x$–$y$ phase relationships, and the complicated connections to the distribution of force coefficients and the wake dynamics (see Section 4) along a flexible cylinder.

## 3.1. Uniform Flows

The pioneering direct numerical simulations (DNSs) by Newman & Karniadakis (1996, 1997), although at a very low Reynolds number, provided evidence of the lock-in response of a cable in a uniform cross-flow, vibrating at a single frequency, with responses that could be based on either standing or traveling waves, depending on the aspect ratio. By increasing the Reynolds number one order of magnitude, Evangelinos & Karniadakis (1999) and Evangelinos et al. (2000) showed that the main VIV physics observed in their previous work remained unperturbed. The strip-theory simulations by Willden & Graham (2004) consisted of a series of planar large eddy simulation regions located at different $z$ positions along the length of a high-aspect-ratio tensioned beam, such as the one depicted in **Figure 1*c***. The flow was resolved in these planar sections and coupled to the structure, resulting in localized excitation planes with less computational cost than full three-dimensional simulations. Willden & Graham (2004) showed that the vibrational response of their flexible cylinder was multimode, with all modes running at the vortex shedding excitation frequency, even though the system was subject to a uniform incoming flow. The authors suggested that added mass allowed the system to respond with a frequency that differed from its natural frequencies, especially when the cylinder had a low mass ratio. The details of how this process was driven were not further investigated because of the limitations posed by the discrete nature of the strip method.

Measuring the VIV of a flexible cylinder model in the laboratory is not an easy task. Having a well-controlled and quality incoming flow in this type of study is crucial. Besides, measurements should allow us to obtain the forces and multimode response, which could include standing and/or traveling waves, in both in-line and cross-flow directions, resulting from vortex shedding excitation, as pointed out by early numerical simulations. One of the first comprehensive laboratory experiments that attempted this type of measurements was conducted by Chaplin et al. (2005b). The authors measured the VIV response of a vertical tensioned cylinder model (similar to the general case shown in **Figure 1*c***) with an external diameter of 28 mm and a total length of approximately 13 m, leading to a relatively high aspect ratio, near 500. Experiments were done by

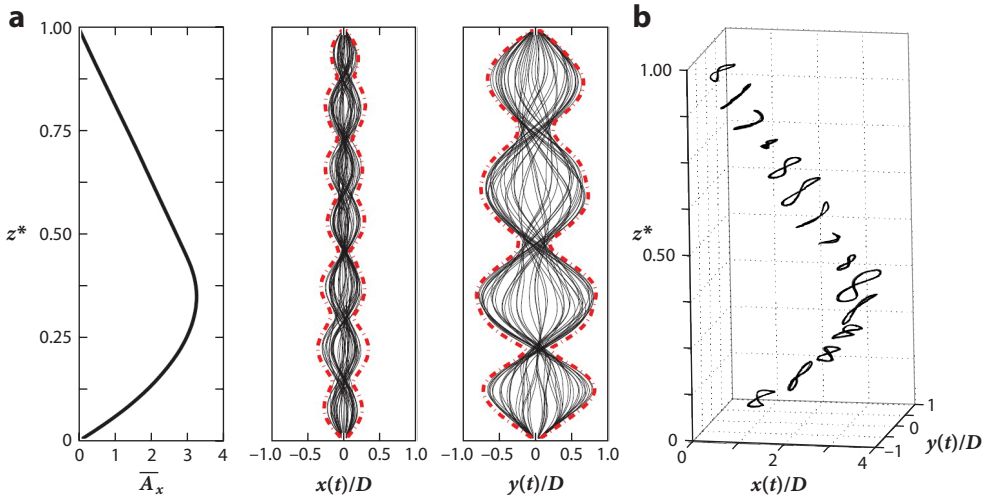


**Figure 2**

Typical results obtained in the experiments by Chaplin et al. (2005b) as presented by Huera-Huarte (2006). (*a*) Mean in-line deflection in dimensionless form $\overline{A_x}$ (*left column*), and in-line $x(t)/D$ (*middle column*) and transverse $y(t)/D$ (*right column*) deflections in dimensionless form, at different instants (*solid lines*) of an experiment. Dashed lines indicate displacement envelopes in the whole experimental run. (*b*) Trajectories in $xy$ planes at different points ($z^* = z/D$) along the model, expressed in dimensionless form [$x(t)/D$ and $y(t)/D$].

varying the incoming flow in very small increments of towing velocity, therefore producing very small changes in the reduced velocity (and Reynolds number) between each experimental run. The natural frequencies of the model were changed by changing the applied tension. A large parameter space was covered, under highly controlled flow and structural conditions, leading to more than 200 experiments. The cylinder, with a low mass ratio of 3, was exposed to a vertical stepped current that implied a uniform flow in its lower half, leaving the upper part in still water (or in air in a few specific cases). Full details of the design used for the experiments, the instrumentation, and the results are provided by Chaplin et al. (2005b) and Huera-Huarte (2006).

The results obtained by Chaplin et al. (2005b) showed, for the first time, highly detailed dynamic responses for a perfectly known incoming flow, with excitations up to the eighth and the fourteenth structural modes of vibration, in the transverse and the in-line direction, respectively. For reference, typical dynamic response results appear in **Figure 2**. The figure shows the displacement data of a single experimental run, where the response was dominated by the seventh mode in-line and the fourth cross-flow. The mean in-line deflection resulting from the mean drag force acting on the structure appears together with the in-line and cross-flow deflections at multiple instants in time (**Figure 2*a***). The same data are presented in a three-dimensional plot, where the trajectories at different locations along the length of the model can be seen (**Figure 2*b***).

The experimental campaign showed that the measured responses were in fact made of contributions from several modes, all running at the same lock-in frequency, and this happened in both directions. This strong lock-in behavior showed responses that grew monotonically with reduced velocity inside each lock-in range, until they suddenly reduced, jumping to the next structural mode of vibration, as in a sawtooth function (see **Figure 3*a***). The plot depicts the spatiotemporal standard deviation of the transverse dimensionless amplitude as a function of reduced velocity, and although the in-line deflections are not shown, they have similar trends. Each dot in the figure results from an experimental run such as the one presented in **Figure 2**. The

**Dimensionless amplitude:** the displacement (in-line or transverse) divided by the diameter, $A^*_{x,y} = x, y/D$

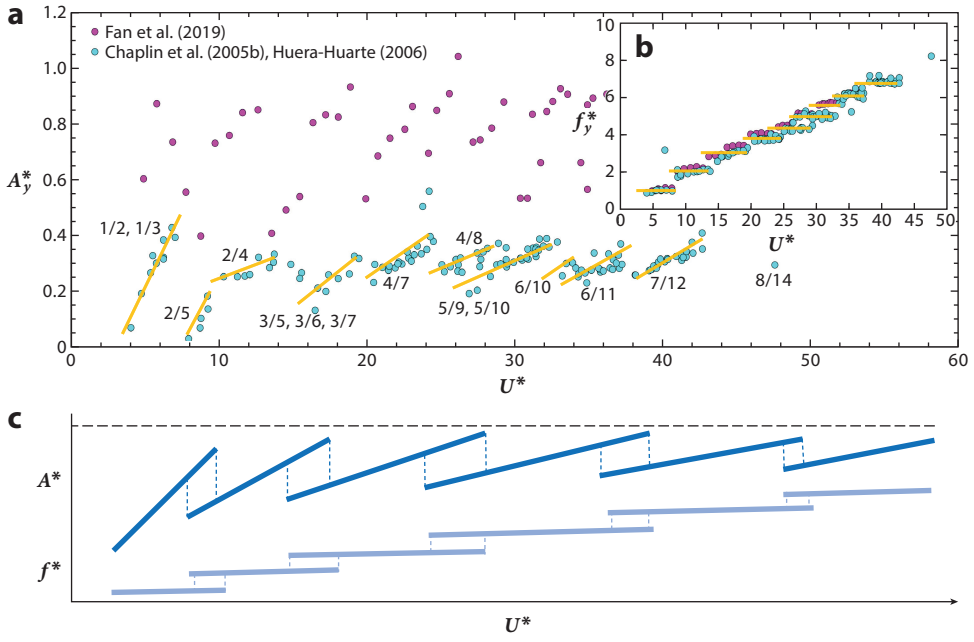


**Figure 3**

Transverse displacements and frequencies of a flexible cylinder in uniform flow as a function of reduced velocity. Amplitudes grow monotonically and appear grouped by modes with certain combinations of transverse/in-line modes. Frequencies grow in a stairway fashion, with the steps indicating the lock-in regions. (*a*) Cyan dots are the spatiotemporal standard deviation ($A_y^*$) of transverse motions from Chaplin et al. (2005b) and Huera-Huarte (2006). Lines are used to indicate the trends associated with the modal combination group that appears in the response. (*b*) Dimensionless dominant cross-flow frequencies, i.e., the responding frequency divided by the natural frequency of the first mode, for the data that appear in panel *a*. (*c*) Sawtooth qualitative representation of the amplitudes of a generic flexible cylinder undergoing vortex-induced vibration in a uniform flow. Vertical dashed lines indicate that there is mode overlapping, and the horizontal dashed line indicates the fact that amplitudes are self-limited. Magenta dots in panels *a* and *b* are maximum transverse displacements of the cylinder and dimensionless frequencies, respectively, in the experiments by Fan et al. (2019).

inclined lines in the plot are used to emphasize the increasing amplitude trend inside each lock-in branch, and the numbers indicate the combination of cross-flow/in-line mode observed. For example, in the range of reduced velocities from 3 to 7, the spatiotemporal standard deviation of the amplitude of the vibration grows linearly from 0.06*D* to 0.45*D*, and the cylinder model showed a response dominated by a combination of the first transverse mode of vibration and either the second or the third in-line mode. At a reduced velocity of 8, experiments start to fall inside the next lock-in branch, which begins with another combination of a cross-flow/in-line mode, again with increasing amplitude. These amplitudes were found to be self-limiting, as lateral deformations need to be accommodated by axial extensibility and stiffness. The maximums of the spatiotemporal standard deviations were near 0.5*D* and the absolute maximums along the length [not shown in the figure (see Huera-Huarte 2006)] slightly exceeded 1*D* in some cases. Dimensionless frequencies were found to be approximately constant inside each lock-in branch (**Figure 3*b***), with a value given by the natural frequency of the lock-in mode, and to jump from one lock-in state to the next in a stairway fashion. Horizontal lines in the plot are used to emphasize this trend. For example, the points in **Figure 3*b*** that fall in the first lock-in branch, with reduced

**Dimensionless frequency:** dominant frequency (in-line or transverse) divided by the natural frequency, $f_{x,y}^* = f_{x,y}/f$

velocities in the range from 3 to 7, have a dimensionless frequency of approximately 1. In the next lock-in branch the dimensionless frequency is 2, and so on. A ratio of 2 to 1 was mainly found between the in-line and the cross-flow frequencies, exhibiting dual resonance, with both the in-line and the cross-flow modes locked in. The appearance of higher harmonics was observed in certain runs. Figure-of-eight trajectories were dominant with phase varying along the length depending on the combination of modes that produced the motion, as appeared in the experiment included in **Figure 2*b***. Results showed clear mode overlapping, with significant contributions from more than two modes, and modal combinations that persisted over a wide range of reduced velocities.

Experiments conducted by Fan et al. (2019) 14 years later, with a flexible cylinder of aspect ratio 240 in uniform flow, showed very similar amplitude–frequency response trends. Maximum dimensionless displacement amplitudes obtained by Fan et al. (2019) have been included in **Figure 3*a*** instead of standard deviations for the sake of clarity. The data show amplitude growth in different groups made of different combinations of dominant cross-flow/in-line responding mode, of the form $2n : n$ and $2n - 1 : n$, as in the data from Chaplin et al. (2005b). The dimensionless frequencies (**Figure 3*b***) appear well grouped in plateaus of approximately constant frequencies as described above. In general, there is good agreement between these two datasets, even though in one of them the incident flow is stepped and in the other it is not. To summarize the major trends observed in this type of problem, a qualitative representation of the amplitude and frequency response found by Chaplin et al. (2005b) and confirmed in the experiments by Fan et al. (2019) has been included in **Figure 3*c***. The plot emphasizes the overall behavior of this type of structure in uniform flows, showing lock-in branches in the amplitude and frequency, mode jumps, overlapping, and the fact that amplitudes are self-limited independently of the mode. In some of these experiments, there were mode switches between adjacent modes during the runs, indicating mode competition in the overlapping regions. Hysteretic behavior related to the mode overlapping phenomena was not investigated, although other authors have shown more recently this possibility in experiments with a low-aspect-ratio cylinder in uniform flow responding with low mode numbers (Gedikli & Dahl 2017). The Chaplin et al. (2005b) dataset included force measurements, demonstrating that the amplitude and frequency were strongly correlated not only with the growth and attenuation of the lock-in process of each mode, but also with the drag forces observed, with clear in-line force amplification (in excess of 120% of the expected stationary cylinder drag) caused by the large amplitudes observed, which could be over $1D$ at the maximum excursion along the length of the model. The drag amplification caused by the resonant response was later studied by Huera-Huarte & Bearman (2009b) and Huang et al. (2011), comparing different expressions to link the amplitude and in-line force. These amplification phenomena are described on a modal basis in the work by Bourguet (2020), although the amplification was not as large as observed in experiments.

More experiments with flexible cylinders in uniform flows (Trim et al. 2005; Huera-Huarte & Bearman 2009a,b; Song et al. 2011; Huera-Huarte et al. 2014; Song et al. 2016; Fan et al. 2019) have confirmed some of the features of the response described above after the work by Chaplin et al. (2005b), including similar in-line to cross-flow amplitude and frequency relationships, force amplification with lock-in response, and $x$–$y$ synchronization patterns. Seyed-Aghazadeh et al. (2019) used optical techniques to reconstruct the VIV dynamics of a highly flexible cylinder in a recirculating water tank. Standing waves with a strong multimode behavior, made of more than four contributing modes, independently of the different boundary conditions investigated, were found. Another common feature was dual resonance, with the appearance of higher harmonics in the in-line response. The main features described in all these experiments hold true even in more

recent cases in which, although the flow was uniform, the cylinder had two different diameters promoting multifrequency excitation (Li et al. 2022).

Additionally, the Chaplin et al. (2005b)/Huera-Huarte (2006) dataset allowed the investigation of the time-dependent fluid force distribution along the axis of the vertical cylinder model undergoing VIV (Huera Huarte et al. 2006). This was done by solving the inverse problem of using the measured response as the input to a structural numerical code based on the finite element method. The authors found that drag distributions followed the shape of the cross-flow deflection, revealing quantitatively a large increase in drag force where the largest cross-flow structural displacement antinodes were found. Local instantaneous drag coefficient values up to 4.5 were found, more than four times those expected in stationary cylinders at the same *Re*. Conversely, at the cross-flow nodes, with almost no response, the values were similar to the ones observed in stationary cylinders. Lift coefficient distribution also followed the modal shape of the cross-flow deflections, with very small values at the nodes and maximum values of up to 5 at the antinodes. Although some hypotheses were made by Huera-Huarte & Bearman (2009b), the question of what type of vortex-shedding structures were generating the observed dynamics and the indirectly computed fluid loading remained unsolved after these experiments. A discussion on this specific matter is presented in Section 4.

The results obtained by Chaplin et al. (2005b)/Huera-Huarte (2006) were also used to conduct a blind prediction exercise, to compare the experimental data obtained with more than 12 simulation tools available from different research groups (Chaplin et al. 2005a). Additionally, several authors have used the data for validation and comparison of different types of numerical simulations using specific experimental runs (see Sun et al. 2012, Wang & Xiao 2016, Lin & Wang 2019, and Pang et al. 2019, just to mention some).

The phenomenon of mode jumping between consecutive modes as reduced velocity is increased, and the modal overlapping, suggested that added mass played a crucial role in self-sustaining the oscillations in a certain mode, over a wide range of vortex shedding excitation. This was later confirmed by Huera-Huarte et al. (2014) with stepped current experiments, where the objective was to compare the response of flexible cylinders with low and very low mass ratios. In the case of the almost neutrally buoyant model investigated, the authors observed wide-banded larger amplitudes of response, with modal contributions consisting of an even larger number of modes. In parallel to all these experimental works, Violette et al. (2007) developed a numerical model by coupling a tensioned cable structural model and a set of wake oscillators distributed along the span of the structure to investigate VIV response in uniform flows. Wake oscillators are based on a differential equation that models the alternating nature of the lift force in the wake of a cylinder (Païdoussis et al. 2014). The oscillators are coupled to a structural model of the bluff body, allowing a simplified representation of the dynamic interaction between the cylinder motion and the vortex shedding. The work by Violette et al. (2007) was based on the authors' previous investigations with rigid cylinders (Facchinetti et al. 2004a) and with a hanging cable in cross-flow (Facchinetti et al. 2004b). The authors demonstrated, by comparison with the DNS results by Newman & Karniadakis (1997), that wake oscillators were an alternative to more expensive simulations in order to study VIV physics, providing a new tool for parametric studies. The model was able to capture not only the modal content of the overall response, but also the standing and traveling waves that appeared in a study with a uniform flow. Later on, Violette et al. (2010) performed linear stability analysis with a similar model and used it to investigate a tensioned beam in uniform flow, comparing the results with the experiments of Chaplin et al. (2005b). The stability analysis demonstrated that mode overlapping was possible, because more than one mode, each with a distinct frequency, was unstable at a certain flow velocity, giving a physical explanation for the previous experimental observations. The appearance or not of this overlapping was explained

through a dimensionless parameter included in the coupled system, referred to as the combined mass number. It was, in fact, the product of dimensionless mass and a parameter included in the wake oscillator equation, which gives the sensitivity of the wake dynamics to the motion of the cylinder, and hence, it indicated the strength of the fluid–structural coupling. The most unstable mode was the one that persisted in the response. Violette et al. (2010) also investigated the mode switching observed experimentally by Chaplin et al. (2005b), concluding that it was the result of cases with two unstable modes that had the same growth rate and therefore could appear indistinctly in the overall response. With similar tools, Grouthier et al. (2013) described the effect of gravity-induced varying tension along the length of a highly flexible free-hanging string in uniform cross-flow at low *Re*. They found standing wave behavior and the appearance of traveling waves only at the highest *Re* investigated. This work proved that at the conditions tested, the spatial distribution of the amplitude of vibrations was self-similar, showing an excellent collapse of the data presented for the different modes when rescaling the spanwise coordinate. Modeling based on the use of wake oscillators has proven to be a successful technique to study the VIV of flexible cylinders in uniform flows, not only to investigate fundamental aspects such as the ones described above, but also because its computational cost is restricted if compared to other simulation techniques; see, for example, the parametric study investigating the capabilities of energy harvesting using the VIV of cables in cross-flow by Antoine et al. (2016) or the study of the dynamics of a flexible cylinder in uniform cross-flow by Srinil (2010), where the author used a tensioned beam model coupled to distributed van der Pol wake oscillators. Cases reported there demonstrated highly modulated amplitude response, multimode lock-in, and mode switching, again indicating that modal responses overlap in specific reduced velocity ranges, with lock-in bandwidths and hydrodynamic added mass coefficients that were mode-dependent, as in the previous experimental observations.

Other numerical techniques have substantially contributed to the understanding of VIV in uniform flows. Highly resolved numerical simulations characterized by a reduced computational cost have recently appeared (Bao et al. 2016, 2019), thanks to a new version of strip theory in which thick strips are used. Still, one of the main problems associated with these simulations is that they are prohibitive when attempting large parametric studies and have been limited to specific cases of interest. The study by Fan et al. (2019) combined highly detailed experiments (see **Figure 3*a*,*b***) and high-fidelity three-dimensional simulations. Interestingly, the simulations presented relate modal overlapping and modal switches to sectional added mass coefficients, something not available before with this degree of detail. The authors also reported inverse computations of hydrodynamic coefficient distributions along their model, confirming important added mass variations along the length, as well as when response changes the dominant mode. In fact, they concluded that the hydrodynamic coefficients observed in the two-degrees-of-freedom VIV of flexibly mounted rigid cylinder experiments by Dahl (2008) are practically the same as those found with flexible cylinders in uniform flows, if similar sectional $x$–$y$ trajectories apply. Moreover, they found that the phase of the motion in the $x$–$y$ plane dictates the values and character of the coefficients. Certain experiments (Huera Huarte et al. 2006, Song et al. 2016) had already linked variations of hydrodynamic coefficients along the length of high-aspect-ratio flexible cylinders with the $x$–$y$ phase distribution, but the analysis presented by Fan et al. (2019) is highly detailed and conclusive. In the same direction, the data obtained from the numerical simulations by Bourguet (2020) give an in-depth view on the relationship between the in-line to cross-flow phase and the regions of either damping or excitation along the length of the cylinder model. The author introduced flow–structure energy transfer maps for different phase trajectories that are described using the Hilbert transform and the analytical signal used to study $x$–$y$ synchronization in the time domain, as previously done by Huera-Huarte & Bearman (2009a).

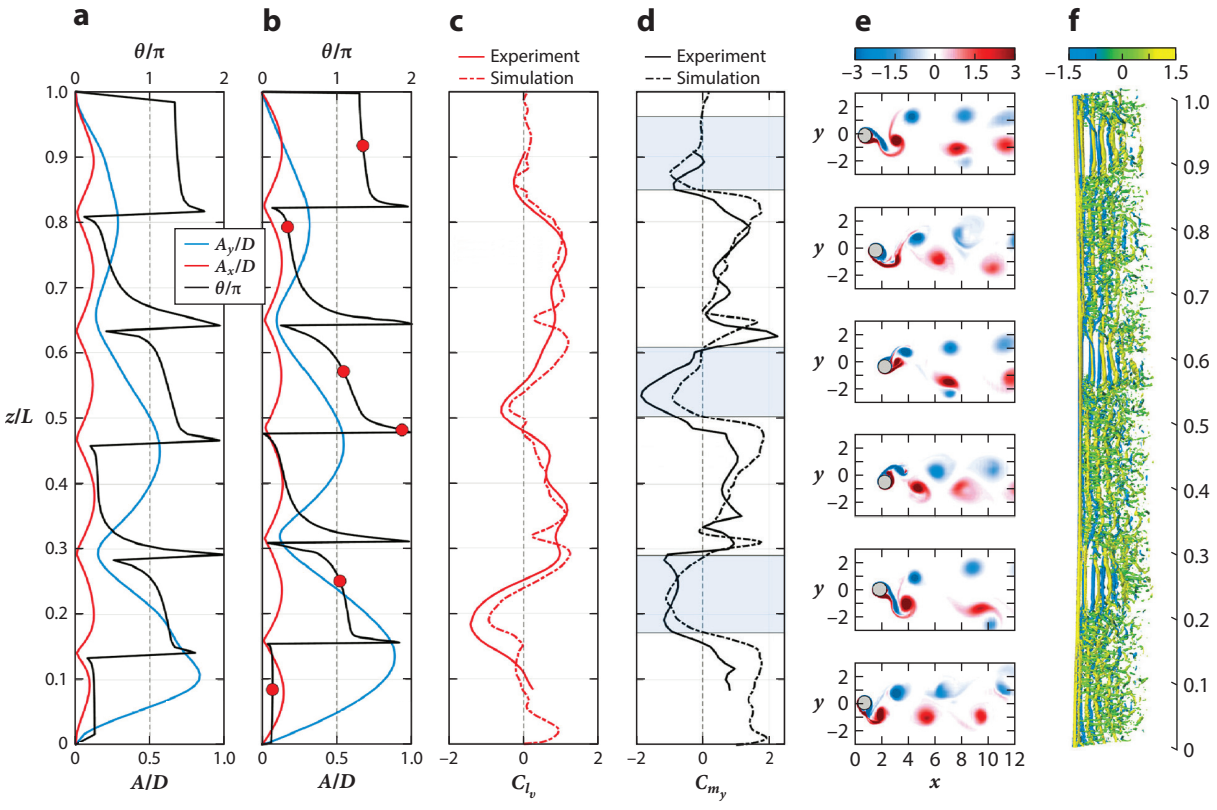


**Figure 4**

Results showing the response, loading, and flow dynamics on a flexible circular cylinder in uniform flow. (*a*) Root mean square of dimensionless in-line (*red*) and cross-flow (*blue*) deflections and *x*–*y* phase (*black*) along a length of the model. (*b*) Numerical simulation of the experimental results in panel *a*, where red dots indicate locations of the planar vorticity fields presented in panel *e*. (*c*) Transverse force coefficient in phase with velocity. (*d*) Transverse added mass coefficient. (*e*) Dimensionless vorticity fields obtained from the simulations at different locations along the length of the model (*red dots* in panel *b*). (*f*) Three-dimensional flow (isosurfaces of vorticity) around the cylinder model obtained from the numerical simulations. Figure adapted with permission from Wang et al. (2021).

Bourguet (2020) identified standing waves mainly in the cross-flow direction, while in the in-line one, standing waves combined with traveling waves in the overall response. The natural continuation of the work by Fan et al. (2019) is that by Wang et al. (2021), who used experiments and simulations to study a flexibly mounted rigid cylinder initially, and later on a flexible cylinder, both in uniform flow. The emphasis of the analysis was given to the investigation of the role of added mass in the overall behavior of the system. For the case of the elastic cylinder, the researchers presented an experimental run that was also numerically simulated (see **Figure 4**), showing excellent agreement. The figure shows the in-line and cross-flow dimensionless root mean square (RMS) amplitude distribution, together with the *x*–*y* phase distribution along the length of their cylinder model (**Figure 4*a*,*b***). The transverse force coefficient in phase with velocity (**Figure 4*c***) and the transverse added mass coefficient (**Figure 4*d***) distributions are also included. The run is for a case responding with mainly standing waves at the third and the sixth cross-flow and in-line modes, respectively. There is a phase jump at every in-line node, and the evolution of the phase between each node and the next is dependent on whether the jump takes place through a cross-flow node

or not. The output of the simulation is scrutinized, showing the strong influence of the phase between the *x–y* motions on the forces acting on the model. A very relevant result is the confirmation that counterclockwise orbits, i.e., *x–y* phases in the range from 0 to $\pi$, imply power-in regions where the transverse force coefficient in phase with velocity is positive. On the other hand, in the regions where the transverse added mass coefficient is negative (the vortex force is out of phase with the motion), the *x–y* phase is in the narrow range from $\pi/2$ to $3\pi/2$.

All these recent numerical works represent a true step forward in the understanding of VIV dynamics in uniform flows, and they confirm many previous observations and hypotheses derived from experiments and other early numerical investigations. The recent application of physics-informed neural networks to the study of VIV in uniform flows (Kharazmi et al. 2021), although incipient, holds promising potential.

## 3.2. Shear Flows

The study of the effects of shear on VIV has received considerably more attention than the case of uniform flow, as it is common in engineering applications even though a priori, because of its nature, it is a more complex problem. Achieving highly controlled uniform or shear flows for high-mode-number VIV research is only possible in laboratories with very specific facilities, such as very large towing tanks, recirculating water channels, and rotating arm facilities. Shear is inherent to almost every field test, as incoming flow conditions cannot be controlled. It implies a variation of the shedding excitation frequency along the length of the cylinder, and intuitively, one should expect excitation of multiple eigenfrequencies at the same time. In terms of amplitude response, there is a clear consensus that incident sheared flows result in amplitudes and curvatures, and therefore fatigue (which is of extreme importance in engineering applications), that are smaller when compared to the case of uniform flows (Trim et al. 2005).

In early field experiments by Kim et al. (1986), a series of important observations were made describing certain aspects of the VIV of long flexible cylinders in shear flow. At the time, most of the data available were for rigid sections of cylinders (as in **Figure 1*b***) under lock-in conditions, and in these experiments, the authors described the behavior of the cylinder as an infinite string, without single-mode lock-in and with reduced drag coefficients if compared to those expected under lock-in conditions. Naturally, one may think that because of shear, a broad-banded response is more likely to occur than in the case of uniform flows, as more modes could be excited, but the available data at that time did not allow researchers to obtain modal content because of the low spatial resolution. Vandiver et al. (2009) investigated the effects of shear in the VIV dynamics of a low-mass-ratio flexible cylinder. The cylinder, with a high aspect ratio, was densely instrumented with fiber-optic strain gauges and towed from a research vessel, while the incoming flow speed was measured using acoustic Doppler techniques. The experiments revealed a clear dominance of traveling waves along the cylinder model. They found a region, extending along the lower 10% of the length of the pipe, where standing waves were found, and outside this region and up to more than half of the length, strong traveling wave behavior was identified. They suggested that the small part where standing waves dominated was the result of incoming and reflecting traveling waves at the bottom end. Based on the orbital trajectories of the cylinder model at different heights along its axis, the authors described how traveling waves evolved in both in-line and cross-flow directions, and if they were phase locked. It was suggested that the transverse force along the length of the pipe was phase locked to vortex shedding, traveling at the same wave speed. With this, one would expect inclined vortex shedding tubes along the length of the pipe, separating in an in-phase fashion with the traveling wave. This work was the continuation of previous research by Vandiver et al. (1996), where some hypotheses for the appearance of lock-in in

highly sheared flow conditions were established. The ability of the structure to lock in at a certain mode was said to be relative to the amount of power available to each mode from the incoming shear and the modal density. A uniform flow and a highly sheared flow were found to be more likely to result in single-mode response than a mild shear. Lock-in is strongly related to modal density, which depends on the aspect ratio and the dynamic characteristics of the structure (see Section 2), and based on these two concepts a map for the likeliness of lock-in to take place was proposed.

Apart from field experiments, there is a dearth of experimental data presenting VIV responses in shear flows stemming from highly resolved and controlled parametric experiments. The generation of a well-known shear profile is not an easy task in the laboratory, as it requires large facilities and specially designed water channels or the use of rotating towing arms in still water. One of the few laboratory experiments that include uniform and shear flow cases (Trim et al. 2005) is centered on describing fatigue characteristics rather than a thorough description of the physical phenomena taking place. Based on the data presented, it is difficult to find large differences in the overall VIV behavior as a result of the shear. In the dataset produced by Lie & Kaasen (2006), the cylinder model exhibited a broad-banded frequency response, mainly built by traveling waves without the appearance of lock-in. These trends became more apparent with increasing flow speed, although, parametrically speaking, the experiments were limited. A novel experiment was carried out recently by Fu et al. (2022), where a flexible cylinder with a low mass ratio (2) and a relatively high aspect ratio (270) was forced to rotate about its center inside a still water tank, generating a bidirectional shear. The existence of standing wave behavior and traveling wave patterns in different experiments is made evident in the spatiotemporal plots presented for specific runs. Interestingly, in this dataset, maximum RMS VIV amplitudes appear grouped by modes, although there is no modal overlapping. Moreover, the data inside each modal group do not follow a clear trend, as in the case of uniform flows where a pattern was observed, indicating monotonically increasing amplitudes (see Section 3.1). The question of this being a result of the existing traveling waves was not discussed by the authors.

In terms of numerical simulations, Newman & Karniadakis (1997) included the study of one case with incoming shear but with a very low *Re*. Amplitude spatiotemporal plots resulting from the simulations could be described by chevron patterns, indicating the presence of traveling waves with changes to standing wave configurations. The sectional lift coefficient was found to be at a maximum where shear velocities were intermediate. Conversely, the correlation of incoming flow velocity and drag was evident. More recent simulations by Bourguet et al. (2011a) have shown standing wave dominance near the ends and confirmed that the response was built on a combination of both standing and traveling waves with incoming shear flow. They also observed single and multifrequency responses along the span of their cylinder model, with lock-in and non-lock-in responses in spanwise regions. These well-differentiated regions formed spanwise cells of drag and lift coefficients controlled by the response patterns of the structure. The authors computed hydrodynamic coefficients, concluding that there was an energy balance between the high-velocity excitation regions, dominated by lock-in, and damping regions outside those. Extended versions of this initial work published by Bourguet et al. (2011b, 2012) revealed again the coexistence of standing and traveling waves in the numerical experiments, in both in-line and cross-flow motions, with frequent changes between the two types of behavior. This happened at all *Re* investigated, in the range of approximately 100 to 1,000. Mono- and multifrequency responses were observed at different spanwise locations in both directions. Lock-in was identified, with clear synchronization between shedding and motion in only one-third of the length of the cylinder, where the high velocity of the incoming shear was imposed. Because the study was limited to three cases,

aspects such as the existence of mode overlapping in the presence of shear remained unclear. The parametric study by Srinil (2011) using wake oscillators shed some light on that matter. The author presented results that indicated multiple peaks and overlapping of modal amplitudes, with responses that revealed the presence of standing waves and combinations of standing–traveling wave response. Further work by Bourguet et al. (2013a) dealt with the effects of the type of shear by comparing linear to exponential functions. Under lock-in conditions, mixed standing–traveling wave responses were found with wider band response and smaller amplitudes in the exponential shear cases. The same authors (Bourguet et al. 2013a) studied synchronization patterns between the in-line and cross-flow motions using Hilbert transforms and the analytical signal concept. Again, they identified the lock-in condition in the region of the cylinder where the incoming flow was at a maximum, with $x$–$y$ phases remaining inside a narrow range, therefore linking certain phases to the excitation region of the cylinder.

Related to the appearance of lock-in, the results presented by Modarres-Sadeghi et al. (2011) from their analysis of experiments conducted inside the Norwegian Deepwater Programme confirmed that VIV oscillations in the presence of shear could be quasi-periodic, chaotic, or combinations of both, in time and space. The chaotic oscillations were observed at different points along the length of the models at different time intervals. The shear promoted the appearance of multiple modes in the response with chaotic oscillations, but the authors commented on the counterbalance effect of the shear-induced traveling waves acting as an energy transfer mechanism between different regions along the cylinder, as in the simulations by Bourguet et al. (2011a). Simulations by Mathelin & de Langre (2005) using distributed van der Pol oscillators had previously indicated the existence of wave packets distributed along the span of their tensioned cable model, which were attributed to local lock-in, where fluid and structure frequencies matched each other. They described how damping had an effect on the envelope of the motion but not on the global behavior of the system. In the same direction, work carried out by Violette et al. (2007) consisted of the simulation of a tensioned beam in shear flow using the same numerical techniques. Results were compared with the DNS of Lucor et al. (2006), capturing dominant standing wave behavior near the ends of the model and a traveling wave away from them, as found previously by other authors.

It is clear from the above discussions that, as happens with uniform flows, the phase between the in-line and cross-flow motions of flexible cylinders is also of extreme importance in the presence of shear, and it can help to explain the appearance of lock-in or not as it is related to the added mass and the distribution of force coefficients. In an analysis of experimental data, Wu et al. (2016) found a direct link between the $x$–$y$ phase angle, and therefore the orbital trajectories of the model, and whether the system was being excited or damped in that region, as suggested by Bourguet et al. (2013b). They showed that counterclockwise trajectories were associated with excitation regions, while clockwise trajectories indicated damping areas, and that the existence or not of traveling waves can indirectly modify these regions by altering the trajectories along the length of the cylinder. Derived from the identification of power-in/power-out regions are the effects of damping, which have been under scrutiny as well, and more importantly the relationship of damping with the existence or not of traveling waves, as well as its combined effect with added mass. Traditionally, since the first VIV studies with one-degree-of-freedom systems (as in **Figure 1*b***), the mass-damping parameter has been used to explain the maxima of VIV amplitudes (Govardhan & Williamson 2002). There have been several efforts in the past to translate the knowledge gained from single-degree-of-freedom systems to the case of flexible ones (Vandiver 2012). Considering the case of an elastic cylinder vibrating in a cross-flow (as in **Figure 1*c***), the time-averaged power input to the system must be the same as the power out (Vandiver et al. 2018); therefore, there must be well-differentiated power-in regions, associated with a lock-in process, and power-out regions

where the flow and the structure are not synchronized, which is directly derived from the study by Bourguet et al. (2013b).

Recently, Ma et al. (2022b) defined two parameters, one that describes the multimode character of the vibration ($\kappa$) and the other to quantify the importance of traveling waves ($\alpha$). Both result from a low-order representation of the structure, based on proper orthogonal decomposition. The mode dominance factor is nothing more than the ratio of the energy of the first eigenmode to the total energy. The parameter $\alpha$ results from comparing the real and the imaginary parts of the eigenvectors. A moving window time domain analysis of the data is performed using the two parameters described. Results are promising and although they need to be extended to larger datasets, they suggest the two parameters can be used to quantify, in a generic way, multimode and traveling wave presence. The $\alpha$ index indicates a strong presence of traveling waves in the shear flow cases studied, emphasizing the idea of clearly distinguishable power-in and power-out regions along the structure, and the transfer mechanism. The mode dominance is highly dependent on the analysis window size used, partly because mode switching can occur.

## 4. THE WAKE BEHIND FLEXIBLE CYLINDERS

Regardless of whether one considers uniform or sheared flows, there is a clear lack of experimental data dealing with the characterization of the wake of flexible cylinders. Applying techniques such as DPIV or flow visualization in high-mode-number VIV experiments is extremely challenging, as it requires very large interrogation regions at different locations along the length of the cylinder models. In fact, to the knowledge of the author, there are no reported DPIV or flow visualization data for high-mode-number VIV experiments conducted in large facilities with low-mass-ratio and high-aspect-ratio cylinder models at high Reynolds numbers.

Van Atta et al. (1988) reported what they called staggered blobs around the nodes of a self-excited high-mass-ratio vibrating wire, at a Reynolds number of 68, using smoke flow visualization. They were the first authors to investigate the spanwise periodicity of the vortex structures downstream from a flexible cylinder when undergoing single-frequency lock-in VIV response. Nevertheless, a complete analysis of the overall flow structures formed in the wake was not carried out. Some suggestions about the nature of the flow structures behind a flexible cylinder oscillating in cross-flow were offered later by several authors (Huera-Huarte 2006, Huera Huarte et al. 2006, Vandiver et al. 2009), but no experimental evidence was provided.

In a flexible cylinder oscillating in standing wave fashion, the amplitude of motion goes from maximum at an antinode, to zero at the node, to another maximum at the next antinode, with the antinodes moving out of phase (see the schematic in **Figure 1*c*** and the data plotted in **Figure 2**). This is considering only the transverse deflection of the system; if the in-line motion is considered as well, in-line nodes appear combined with cross-flow antinodes (see **Figure 2*a***). Huera-Huarte (2006) and Huera Huarte et al. (2006) raised the question of how the vortex shedding could evolve from one antinode to the next in antiphase, through the node, as the shedding had to change phase at the node. In experiments by Huera-Huarte & Bearman (2009b), it was found that the vortex modes in the wake of an oscillating flexible cylinder were dependent on the amplitude distribution along the length of the model. DPIV was used to interrogate the near wake of the cylinder. According to the vortex structure designation introduced by Williamson & Govardhan (2004), the 2S (a single vortex shed at each side of the wake per cycle) mode was dominant and the 2P (a pair of counterrotating vortices shed at each side of the wake per cycle) mode appeared and vanished intermittently in the regions of the model where the largest $x$–$y$ synchronized motions were observed (Huera-Huarte & Bearman 2009a). Further analyses of this DPIV dataset using proper orthogonal decomposition combined with fuzzy clustering

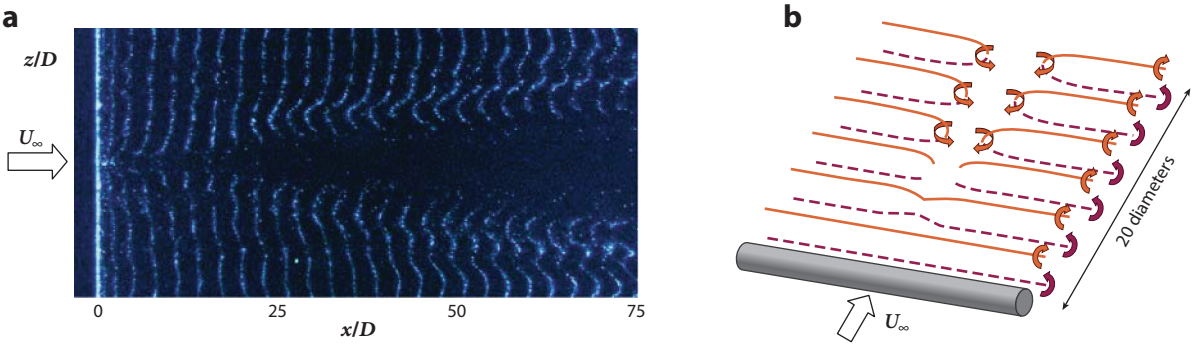


**Figure 5**

The study by Gilbert & Sigurdson (2010) with a long cable in uniform cross-flow. (*a*) Hydrogen bubble flow visualization around a node of the cylinder while undergoing vortex-induced vibration, depicting what the authors defined as the void structure in the wake. (*b*) Vortex skeleton proposed by the authors, showing a vortex pinch-off process connecting opposite signed vortices from each side of the wake, used to explain the void structure observed in the experiments. Figure adapted with permission from Gilbert & Sigurdson (2010).

techniques concluded that the 2P mode was not consistent spatiotemporally (Huera-Huarte & Vernet 2010). The cylinder model in these experiments had a low aspect ratio (≈100), and even with a low mass-damping parameter, only the first two modes of vibration were excited, because of its low modal density. Although the wake was visualized using DPIV, the question of how the vortex shedding transitioned from one antinode to the next remained unanswered. With this limited knowledge related to the structures in the wake of flexible cylinders, Gilbert & Sigurdson (2010) conducted an experiment that tried to shed some light on the problem. The experiment was inspired by the work of Van Atta et al. (1988) and is the first article showing what they defined as the void structure, a region in the near wake where no vortices were observed. Using hydrogen bubble flow visualization (**Figure 5*a***), the authors suggested a vortex skeleton that included a pinch-off (**Figure 5*b***) between opposite-sign vortices at each side of the wake. The void structure was associated with the nodes of the vibrating cylinder, and the authors hypothesized that this type of structure could be observed only in flexible cylinders, due to the appearance of nodes and antinodes and as a result of the oscillatory phenomena, discarding the possibility of perturbations such as imperfections in the surface of the model or others as the origin.

Bangash & Huera-Huarte (2015) constructed a forced vibration experiment with the objective to study the flow structures in the transitional region between two out-of-phase antinodes. They towed a cylinder in still water being forced to move with a mode shape corresponding to the second mode, therefore showing two antinodes at both sides of a node. The frequency of the imposed motion was in accordance with that expected of the self-excited frequency that would result from the towing flow speed. The experiments were inspired by the results presented by Huera Huarte et al. (2006), who found that the instantaneous values of the total lift coefficient were near zero at the nodes, implying some sort of symmetric flow structures dominating the wake at the nodes. Using hydrogen bubble seeding, optical flow, and proper orthogonal decomposition techniques, the researchers obtained flow visualization and DPIV results that confirmed the existence of persisting out-of-phase 2S structures at the antinodes (plots 9 to 24 in **Figure 6*a***) and an elongated symmetric structure at the node, made of two counterrotating vortices that remained attached to the cylinder without shedding (plots 1 to 8 in **Figure 6*a***), as in the void structure of Gilbert & Sigurdson (2010). Hence, at the node, the lack of the

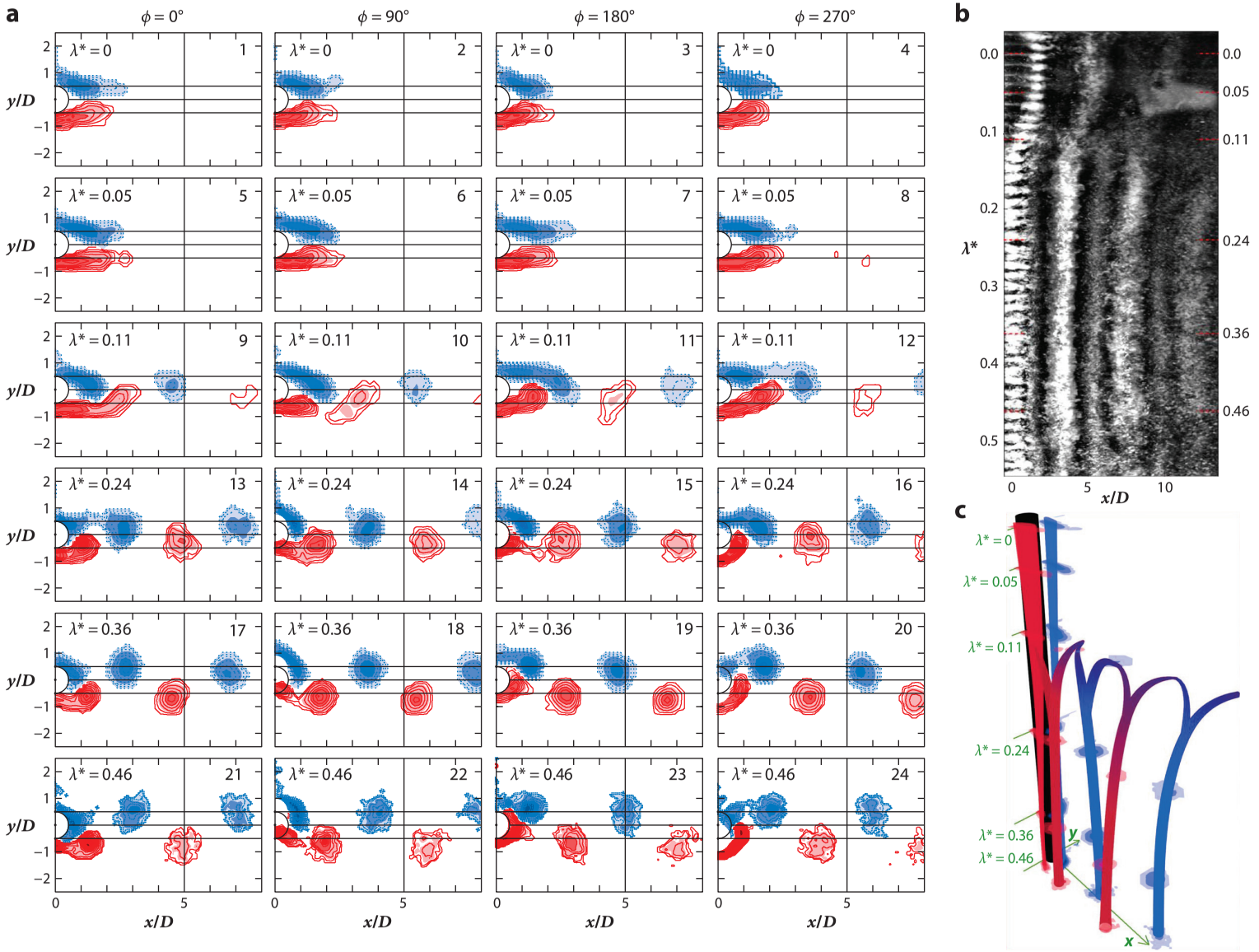


(*Caption appears on following page*)

**Figure 6** (*Figure appears on preceding page*)

Wake structures around the node of the forced vibration experiments by Bangash & Huera-Huarte (2015). (*a*) Digital particle image velocimetry (DPIV) results at different dimensionless heights ($\lambda^*$), in rows, from the node ($\lambda^* = 0$) to one of the antinodes ($\lambda^* = 0.46$), for phases ($\phi$) of 0, 90, 180, and 270° of the shedding process, in columns. (*b*) Flow visualization of the node to antinode transitional region in a longitudinal plane. (*c*) Vortex skeleton reconstruction, showing the planar DPIV results, with the three-dimensional representation of structures observed in the wake. Figure adapted with permission from Bangash & Huera-Huarte (2015).



characteristic opposing shear layer interaction in cylinder wakes resulted in the absence of vortex shedding, and conditions existed such that the vortex shedding underwent a 180° phase shift. A three-dimensional flow skeleton reconstruction (**Figure 6*c***) was proposed after interrogating the flow at multiple transverse (**Figure 6*a***) and longitudinal planes (**Figure 6*b***). The work by Bangash & Huera-Huarte (2015) includes detailed information on the pinch-off process previously suggested by Gilbert & Sigurdson (2010), where a vortex reconnection was observed in the near wake.

Despite the emergence of new experimental three-dimensional techniques, literature addressing the empirical identification of flow structures in the wake of long flexible cylinders remains exceedingly scarce. Advancements are being made, thanks to novel simulations that are playing a crucial role in bridging this gap (Bourguet et al. 2011c, 2012; Bourguet & Triantafyllou 2015; Fan et al. 2019). The simulations by Newman & Karniadakis (1996, 1997) and Evangelinos & Karniadakis (1999) were the first to provide evidence of the three-dimensional nature of the wake of a flexible cylinder in both uniform and shear flows. When cylinders responded with standing waves, they observed two sheets of spanwise vorticity forming what they called an interwoven pattern. Conversely, with the appearance of traveling waves, the shedding was made of oblique tubes that dominated the wake. They found a strong correlation between fluid loading and wake structures, where large lift coefficients were associated with standing wave responses. Quasi-three-dimensional methods (Meneghini et al. 2004; Willden & Graham 2004; Sun et al. 2012; Bao et al. 2016, 2019) have not been able to provide in-depth three-dimensional details on the complexities of the near wake of flexible cylinders. The first highly detailed flow descriptions (Bourguet et al. 2011b,c, 2012; Bourguet 2020) have been derived from DNS of the incompressible Navier–Stokes equations using spectral element methods (Karniadakis & Sherwin 2005) involving uniform and shear flows. **Figure 7*a*** shows the isosurfaces of dimensionless vorticity in a numerical experiment with a sheared flow profile. In general, the shedding is oblique as imposed by the mean deflected shape of the cylinder. On the right-hand side of the panel, the vortex shedding frequency along the length of the cylinder is plotted in parallel to the lift coefficient in phase with velocity, indicating the lock-in region where the power input (with the positive coefficient indicated) takes place. Outside the lock-in region, there are vortex-splitting events with spanwise cells that have a length that correlates to half the cross-flow vibration wavelength. These cells have been observed in the more recent simulations by Fan et al. (2019) and Wang et al. (2021). In **Figure 4*f***, three-dimensional structures (isosurfaces of dimensionless vorticity) are included together with two-dimensional slices (**Figure 4*e***) at different points (marked in the phase plots of **Figure 4*a*,*b***) along the length of a cylinder exposed to uniform flow. The dominant structure is 2S, although it is combined with small regions in which a vortex structure consisting of a single vortex at one side of the wake and a pair at the other [P+S, according to Williamson & Govardhan (2004)] dominates. The latter appears clearly linked to a negative transverse added mass coefficient, meaning that vortex forces are in opposition to the motion. This large change in the added mass coefficient is justified by a sudden change in the vortex structure at the node and a phase shift, as shown by Fan et al. (2019) (see **Figure 7*b***), and as suggested by the work of Gilbert & Sigurdson (2010) and Bangash & Huera-Huarte (2015).

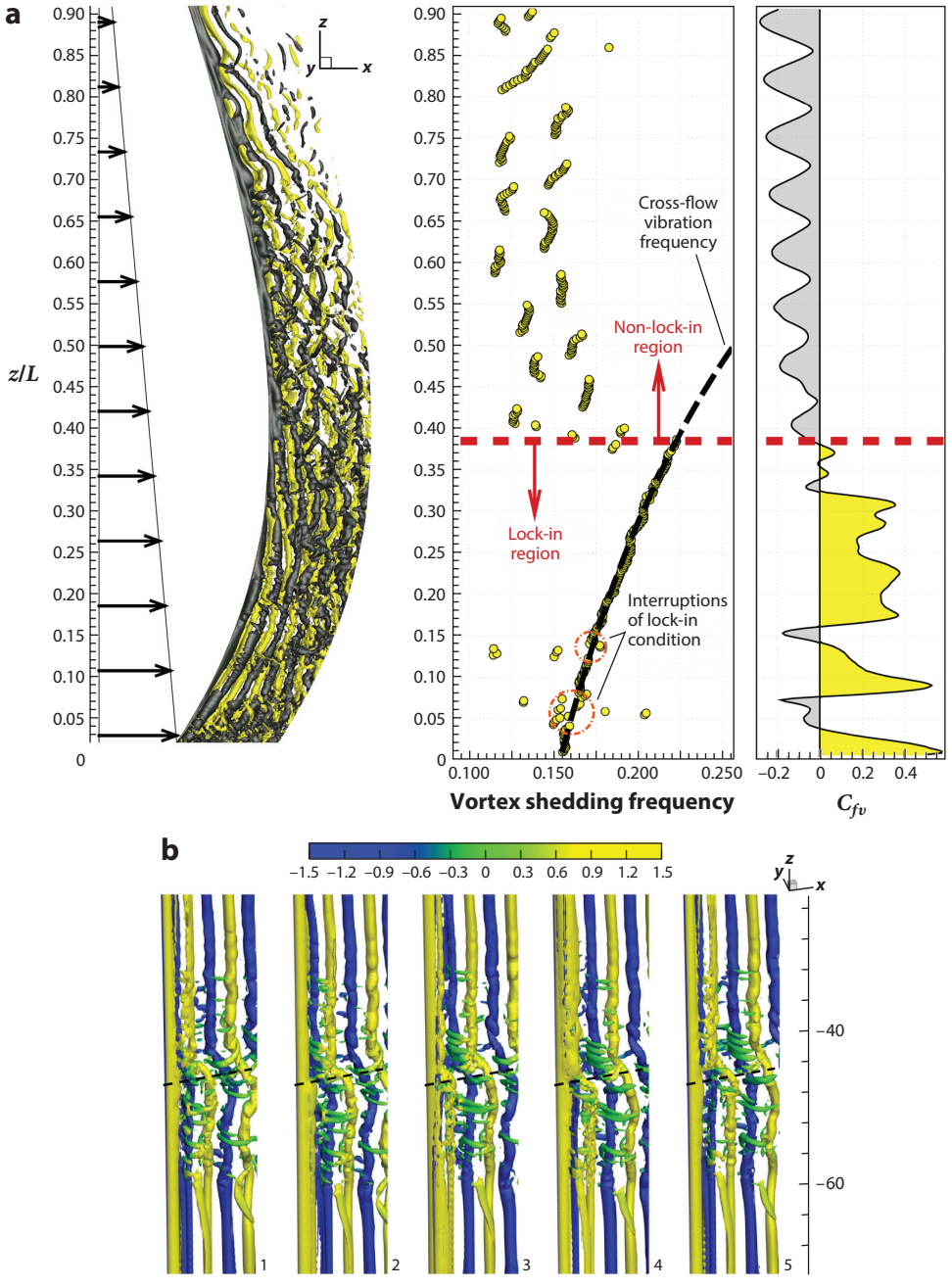


**Figure 7**

(*a*) Isosurfaces of the vorticity in the wake of a flexible cylinder in shear flow (*left column*), vortex shedding frequency along the length of the cylinder (*middle column*), and transverse force coefficient in phase with velocity (*right column*). The dashed line separates the lock-in region, correlated to the higher velocities in the incoming shear and to the positive values of the transverse force coefficient (*yellow*). Panel adapted with permission from Bourguet et al. (2011c). (*b*) Detail of the flow evolution around a node (*dashed line*) of a flexible cylinder undergoing vortex-induced vibration in a uniform flow. Panel adapted with permission from Fan et al. (2019).

## SUMMARY POINTS

1. In uniform flows, vortex-induced vibration (VIV) responses are made of contributions of several modes, locked in at a frequency near that of shedding, and coupled to one of the natural frequencies of the structure. Dual resonance takes place with modal combinations of in-line/cross-flow mode of the form $2n/n$ or $2n - 1/n$. Inside each group, the response grows monotonically until the next group appears.
2. Amplitudes of VIV in flexible cylinders are self-limiting with maximum values near one diameter and spatiotemporal metrics on the order of half a diameter.
3. VIV response is characterized by mode overlapping. The dominant modes in the response are the most unstable, and mode switches can take place between highly unstable modes.
4. Recent experiments with shear flows, though showing lock-in responses at certain specific mode combinations, do not show clear amplitude–frequency trends. Response amplitudes tend to be smaller than in the case of uniform flows.
5. A standing wave response is more likely to appear in uniform or highly sheared flows. Mild shear promotes the appearance of traveling waves away from the ends of the cylinder.
6. Orbital trajectories and $x$–$y$ phases are crucial to understanding hydrodynamic loading, damping, and added mass distribution along the length of flexible cylinders. They govern where power-in and power-out regions are located and what flow structures appear in the wake. In the case of shear flows, power-in regions correlate with high incoming flow velocities, and traveling waves play a crucial role in defining phases.

## FUTURE ISSUES

1. There is a need for highly resolved and controlled experimental results, covering large parametric spaces, for the case of shear flows.
2. Parametric experimental studies to investigate hydrodynamic loading and added mass distribution in high-Reynolds-number flows are needed to complement the recent advances made using numerical simulations at relatively low Reynolds numbers.
3. There is a need for experimental three-dimensional characterization of wakes at higher Reynolds numbers, although recent numerical simulations are starting to provide highly detailed flow dynamics in the wake of flexible cylinders.
4. Emerging methodologies reliant on artificial intelligence and machine learning algorithms are currently in their initial states of development and are in need of high-quality datasets to advance the comprehension of this fluid–structure interaction problem to the next level.

## DISCLOSURE STATEMENT

The author is not aware of any affiliations, memberships, funding, or financial holdings that might be perceived as affecting the objectivity of this review.

## ACKNOWLEDGMENTS

The author gratefully acknowledges the funding provided by the Spanish Agencia Estatal de Investigación (AEI) through grant PID2021-128441NB-I00.

## LITERATURE CITED

Antoine G, de Langre E, Michelin S. 2016. Optimal energy harvesting from vortex-induced vibrations of cables. *Proc. R. Soc. A* 472(2195):20160583

Bangash Z, Huera-Huarte F. 2015. On the flow around the node to anti-node transition of a flexible cylinder undergoing vortex-induced vibrations. *Phys. Fluids* 27(6):065112

Bao Y, Palacios R, Graham M, Sherwin S. 2016. Generalized thick strip modelling for vortex-induced vibration of long flexible cylinders. *J. Comput. Phys.* 321:1079–97

Bao Y, Zhu HB, Huan P, Wang R, Zhou D, et al. 2019. Numerical prediction of vortex-induced vibration of flexible riser with thick strip method. *J. Fluids Struct.* 89:166–73

Bearman P. 2011. Circular cylinder wakes and vortex-induced vibrations. *J. Fluids Struct.* 27(5–6):648–58

Bearman PW. 1984. Vortex shedding from oscillating bluff bodies. *Annu. Rev. Fluid Mech.* 16:195–222

Blevins R. 1990. *Flow-Induced Vibration*. New York: Van Nostrand Reinhold

Bourguet R. 2020. Vortex-induced vibrations of a flexible cylinder at subcritical Reynolds number. *J. Fluid Mech.* 902:R3

Bourguet R, Karniadakis GE, Triantafyllou MS. 2011a. Lock-in of the vortex-induced vibrations of a long tensioned beam in shear flow. *J. Fluids Struct.* 27(5–6):838–47

Bourguet R, Karniadakis GE, Triantafyllou MS. 2011b. Vortex-induced vibrations of a long flexible cylinder in shear flow. *J. Fluid Mech.* 677:342–82

Bourguet R, Karniadakis GE, Triantafyllou MS. 2013a. Multi-frequency vortex-induced vibrations of a long tensioned beam in linear and exponential shear flows. *J. Fluids Struct.* 41:33–42

Bourguet R, Karniadakis GE, Triantafyllou MS. 2013b. Phasing mechanisms between the in-line and cross-flow vortex-induced vibrations of a long tensioned beam in shear flow. *Comput. Struct.* 122:155–63

Bourguet R, Lucor D, Triantafyllou MS. 2012. Mono- and multi-frequency vortex-induced vibrations of a long tensioned beam in shear flow. *J. Fluids Struct.* 32:52–64

Bourguet R, Modarres-Sadeghi Y, Karniadakis GE, Triantafyllou MS. 2011c. Wake-body resonance of long flexible structures is dominated by counterclockwise orbits. *Phys. Rev. Lett.* 107(13):134502

Bourguet R, Triantafyllou MS. 2015. Vortex-induced vibrations of a flexible cylinder at large inclination angle. *Philos. Trans. R. Soc. A* 373(2033):20140108

Bur. Ocean Energy Manag. 2019. *Deepwater Gulf of Mexico report 2019*. OCS Rep. BOEM 2021-005, US Dep. Inter., New Orleans, LA

Chaplin JR, Bearman PW, Cheng Y, Fontaine E, Graham JMR, et al. 2005a. Blind predictions of laboratory measurements of vortex-induced vibrations of a tension riser. *J. Fluids Struct.* 21(1):25–40

Chaplin JR, Bearman PW, Huera-Huarte FJ, Pattenden RJ. 2005b. Laboratory measurements of vortex-induced vibrations of a vertical tension riser in a stepped current. *J. Fluids Struct.* 21(1):3–24

Dahl JM. 2008. *Vortex-induced vibration of a circular cylinder with combined in-line and cross-flow motion*. PhD Thesis, Mass. Inst. Technol., Cambridge, MA

Evangelinos C, Karniadakis GE. 1999. Dynamics and flow structures in the turbulent wake of rigid and flexible cylinders subject to vortex-induced vibrations. *J. Fluid Mech.* 400:91–124

Evangelinos C, Lucor D, Karniadakis G. 2000. DNS-derived force distribution on flexible cylinders subject to vortex-induced vibration. *J. Fluids Struct.* 14(3):429–40

Facchinetti M, de Langre E, Biolley F. 2004a. Coupling of structure and wake oscillators in vortex-induced vibrations. *J. Fluids Struct.* 19(2):123–40

Facchinetti ML, de Langre E, Biolley F. 2004b. Vortex-induced travelling waves along a cable. *Eur. J. Mech. B Fluids* 23(1):199–208

Fan D, Wang Z, Triantafyllou MS, Karniadakis GE. 2019. Mapping the properties of the vortex-induced vibrations of flexible cylinders in uniform oncoming flow. *J. Fluid Mech.* 881:815–58

Fu X, Fu S, Ren H, Xie W, Xu Y, et al. 2022. Experimental investigation of vortex-induced vibration of a flexible pipe in bidirectionally sheared flow. *J. Fluids Struct.* 114:103722

Gedikli ED, Dahl JM. 2017. Mode excitation hysteresis of a flexible cylinder undergoing vortex-induced vibrations. *J. Fluids Struct.* 69:308–22

Gilbert S, Sigurdson L. 2010. The 'void' structure in the wake of a self-oscillating flexible circular cylinder. *Exp. Fluids* 48(3):461–71

Govardhan R, Williamson CH. 2002. Resonance forever: existence of a critical mass and an infinite regime of resonance in vortex-induced vibration. *J. Fluid Mech.* 473:147–66

Grouthier C, Michelin S, Modarres-Sadeghi Y, de Langre E. 2013. Self-similar vortex-induced vibrations of a hanging string. *J. Fluid Mech.* 724:R2

Han SM, Benaroya H, Wei T. 1999. Dynamics of tranversely vibrating beams using four engineering theories. *J. Sound Vib.* 225(5):935–88

Huang S, Khorasanchi M, Herfjord K. 2011. Drag amplification of long flexible riser models undergoing multi-mode VIV in uniform currents. *J. Fluids Struct.* 27(3):342–53

Huera-Huarte FJ. 2006. *Multi-mode vortex-induced vibrations of a flexible circular cylinder*. PhD Thesis, Imp. Coll. Lond., UK

Huera-Huarte FJ, Bangash ZA, González LM, Gonzalez LM, Huera-Huarte FJ, et al. 2014. Towing tank experiments on the vortex-induced vibrations of low mass ratio long flexible cylinders. *J. Fluids Struct.* 48:81–92

Huera-Huarte FJ, Bearman PW. 2009a. Wake structures and vortex-induced vibrations of a long flexible cylinder—Part 1: dynamic response. *J. Fluids Struct.* 25(6):969–90

Huera-Huarte FJ, Bearman PW. 2009b. Wake structures and vortex-induced vibrations of a long flexible cylinder—Part 2: drag coefficients and vortex modes. *J. Fluids Struct.* 25(6):991–1006

Huera Huarte FJ, Bearman PW, Chaplin JR. 2006. On the force distribution along the axis of a flexible circular cylinder undergoing multi-mode vortex-induced vibrations. *J. Fluids Struct.* 22(6–7):897–903

Huera-Huarte FJ, González LM. 2013. Numerical prediction of the modal response of flexible cylinders in cross-flow with a current dependent form of damping. *J. Mar. Sci. Technol.* 18(3):370–80

Huera-Huarte FJ, Vernet A. 2010. Vortex modes in the wake of an oscillating long flexible cylinder combining POD and fuzzy clustering. *Exp. Fluids* 48(6):999–1013

Karniadakis G, Sherwin S. 2005. *Spectral/hp Element Methods for Computational Fluid Dynamics*. Oxford, UK: Oxford Univ. Press. 2nd ed.

Kharazmi E, Fan D, Wang Z, Triantafyllou MS. 2021. Inferring vortex induced vibrations of flexible cylinders using physics-informed neural networks. *J. Fluids Struct.* 107:103367

Kim YH, Vandiver JK, Holler R. 1986. Vortex-induced vibration and drag coefficients of long cables subjected to sheared flows. *J. Energy Resour. Technol.* 108(1):77–83

Larsen C, Vikestad K, Yttervik R, Passano E. Baarholm G. 2005. *VIVANA Theory Manual*. Trondheim, Nor.: Marintek

Li A, Mentzelopoulos A, Triantafyllou MS, Fan D. 2022. Dual-frequency vortex-induced vibrations of long flexible stepped cylinders. *Phys. Fluids* 34(7):075105

Lie H, Kaasen K. 2006. Modal analysis of measurements from a large-scale VIV model test of a riser in linearly sheared flow. *J. Fluids Struct.* 22(4):557–75

Lin K, Wang J. 2019. Numerical simulation of vortex-induced vibration of long flexible risers using a SDVM-FEM coupled method. *Ocean Eng.* 172:468–86

Lucor D, Mukundan H, Triantafyllou MS. 2006. Riser modal identification in CFD and full-scale experiments. *J. Fluids Struct.* 22(6–7):905–17

Ma L, Lin K, Fan D, Wang J, Triantafyllou MS. 2022a. Flexible cylinder flow-induced vibration. *Phys. Fluids* 34(1):011302

Ma L, Resvanis TL, Vandiver JK. 2022b. The influence of mode dominance and traveling waves on flexible cylinder flow-induced vibration. *Ocean Eng.* 264:111750

Mathelin L, de Langre E. 2005. Vortex-induced vibrations and waves under shear flow with a wake oscillator model. *Eur. J. Mech. B Fluids* 24(4):478–90

Meneghini JR, Saltara F, Fregonesi RDA, Yamamoto CT, Casaprima E, Ferrari JA. 2004. Numerical simulations of VIV on long flexible cylinders immersed in complex flow fields. *Eur. J. Mech. B Fluids* 23(1):51–63

Modarres-Sadeghi Y, Chasparis F, Triantafyllou MS, Tognarelli M, Beynet P. 2011. Chaotic response is a generic feature of vortex-induced vibrations of flexible risers. *J. Sound Vib.* 330(11):2565–79
Mukundan H, Hover FS, Triantafyllou MS. 2010. A systematic approach to riser VIV response reconstruction. *J. Fluids Struct.* 26(5):722–46
Naudascher E, Rockwell D. 2005. *Flow-Induced Vibrations: An Engineering Guide.* Mineola, NY: Dover
Newman D, Karniadakis GE. 1996. Simulations of flow over a flexible cable: a comparison of forced and flow-induced vibration. *J. Fluids Struct.* 10(5):439–53
Newman D, Karniadakis GE. 1997. A direct numerical simulation study of flow past a freely vibrating cable. *J. Fluid Mech.* 344:95–136
Païdoussis M, Price S, de Langre E. 2014. *Fluid-Structure Interactions: Cross-Flow-Induced Instabilities*. Cambridge, UK: Cambridge Univ. Press
Pang J, Zhu B, Zong Z. 2019. A numerical simulation model for the vortex induced vibration of flexible risers using dynamic stiffness matrices. *Ocean Eng.* 178:306–20
Sanaati B, Kato N. 2012. A study on the effects of axial stiffness and pre-tension on VIV dynamics of a flexible cylinder in uniform cross-flow. *Appl. Ocean Res.* 37:198–210
Sarpkaya T. 2004. A critical review of the intrinsic nature of vortex-induced vibrations. *J. Fluids Struct.* 19(4):389–447
Seyed-Aghazadeh B, Edraki M, Modarres-Sadeghi Y. 2019. Effects of boundary conditions on vortex-induced vibration of a fully submerged flexible cylinder. *Exp. Fluids* 60(3):38
Seyed-Aghazadeh B, Modarres-Sadeghi Y. 2016. Reconstructing the vortex-induced-vibration response of flexible cylinders using limited localized measurement points. *J. Fluids Struct.* 65:433–46
Shang JK, Stone HA, Smits AJ. 2014. Vortex and structural dynamics of a flexible cylinder in cross-flow. *Phys. Fluids* 26(5):053605
Song JN, Lu L, Teng B, Park HI, Tang GQ, Wu H. 2011. Laboratory tests of vortex-induced vibrations of a long flexible riser pipe subjected to uniform flow. *Ocean Eng.* 38(11–12):1308–22
Song L, Fu S, Cao J, Ma L, Wu J. 2016. An investigation into the hydrodynamics of a flexible riser undergoing vortex-induced vibration. *J. Fluids Struct.* 63:325–50
Srinil N. 2010. Multi-mode interactions in vortex-induced vibrations of flexible curved/straight structures with geometric nonlinearities. *J. Fluids Struct.* 26(7–8):1098–122
Srinil N. 2011. Analysis and prediction of vortex-induced vibrations of variable-tension vertical risers in linearly sheared currents. *Appl. Ocean Res.* 33(1):41–53
Sun L, Zong Z, Dong J, Dong GH, Liu CF. 2012. Stripwise discrete vortex method for VIV analysis of flexible risers. *J. Fluids Struct.* 35:21–49
Triantafyllou M, Triantafyllou G, Tein DYS, Ambrose BD. 1999. *Pragmatic riser VIV analysis*. Paper presented at the Offshore Technology Conference, Houston, TX, May. **https://doi.org/10.4043/10931-MS**
Trim AD, Braaten H, Lie H, Tognarelli MA. 2005. Experimental investigation of vortex-induced vibration of long marine risers. *J. Fluids Struct.* 21(3):335–61
Van Atta CW, Gharib M, Hammache M. 1988. Three-dimensional structure of ordered and chaotic vortex streets behind circular cylinders at low Reynolds numbers. *Fluid Dyn. Res.* 3(1–4):127–32
Vandiver J. 1993. Dimensionless parameters important to the prediction of vortex-induced vibration of long, flexible cylinders in ocean currents. *J. Fluids Struct.* 7(5):423–55
Vandiver J. 2003. *SHEAR7 User Guide*. Cambridge, MA: Mass. Inst. Technol. Dep. Ocean Eng.
Vandiver JK. 2012. Damping parameters for flow-induced vibration. *J. Fluids Struct.* 35:105–19
Vandiver JK, Allen D, Li L. 1996. The occurrence of lock-in under highly sheared conditions. *J. Fluids Struct.* 10(5):555–61
Vandiver JK, Jaiswal V, Jhingran V. 2009. Insights on vortex-induced, traveling waves on long risers. *J. Fluids Struct.* 25(4):641–53
Vandiver JK, Jong JY. 1987. The relationship between in-line and cross-flow vortex-induced vibration of cylinders. *J. Fluids Struct.* 1(4):381–99
Vandiver JK, Ma L, Rao Z. 2018. Revealing the effects of damping on the flow-induced vibration of flexible cylinders. *J. Sound Vib.* 433:29–54
Violette R, de Langre E, Szydlowski J. 2007. Computation of vortex-induced vibrations of long structures using a wake oscillator model: comparison with DNS and experiments. *Comput. Struct.* 85(11–14):1134–41

Violette R, de Langre E, Szydlowski J. 2010. A linear stability approach to vortex-induced vibrations and waves. *J. Fluids Struct.* 26(3):442–66

Wang E, Xiao Q. 2016. Numerical simulation of vortex-induced vibration of a vertical riser in uniform and linearly sheared currents. *Ocean Eng.* 121:492–515

Wang Z, Fan D, Triantafyllou MS. 2021. Illuminating the complex role of the added mass during vortex induced vibration. *Phys. Fluids* 33(8):085120

Willden RH, Graham JR. 2004. Multi-modal Vortex-Induced Vibrations of a vertical riser pipe subject to a uniform current profile. *Eur. J. Mech. B Fluids* 23(1):209–18

Willert CE, Gharib M. 1991. Digital particle image velocimetry. *Exp. Fluids* 10(4):181–93

Williamson C, Govardhan R. 2004. Vortex-induced vibrations. *Annu. Rev. Fluid Mech.* 36:413–55

Wu J, Lie H, Larsen CM, Liapis S, Baarholm R. 2016. Vortex-induced vibration of a flexible cylinder: interaction of the in-line and cross-flow responses. *J. Fluids Struct.* 63:238–58

Xie G, Thompson DJ, Jones CJC. 2004. Mode count and modal density of structural systems: relationships with boundary conditions. *J. Sound Vib.* 274(3–5):621–51